


Flame Flickering can Cease Under Normal Gravity and Atmospheric Pressure in a Horizontally Moving Dual Burner System

Xiaoyu Ju , Anek Bunkwang, Takuya Yamazaki , Tsuneyoshi Matsuoka , and Yuji Nakamura*
Department of Mechanical Engineering, Toyohashi University of Technology, Toyohashi 441-8580, Japan

 (Received 13 August 2022; revised 20 October 2022; accepted 23 November 2022; published 23 January 2023)

This paper provides a feasible way to suppress flame flickering under normal gravity and atmospheric pressure without changing the fuel mass burning rate, thus promoting steady-state combustion. By periodically reciprocating one burner horizontally in a dual burner system, a death mode (namely, amplitude death of flame height oscillation) is generated around the critical burner separation distance, which is a transition point between in-phase and antiphase flickering modes of the two flames. The criterion to obtain a complete death mode region in a general dual burner system (with horizontal movement function) is defined by two dimensionless parameters, which respectively quantify the burner configuration and its dynamic performance.

DOI: [10.1103/PhysRevApplied.19.014060](https://doi.org/10.1103/PhysRevApplied.19.014060)

I. INTRODUCTION

The oscillation and synchronization of buoyant diffusion flames (namely, limit-cycle oscillators) are two typical cases in nonlinear science, and have been studied both theoretically and experimentally [1–8]. When the individual flames in a multi-flame system are distant from each other, each flame is regarded as a single flame and analyzed as such. However, the flames start to synchronize with one another and exhibit a coupled oscillatory behavior termed “puffing” or “flickering” [9] when close to each other, namely, a periodic formation and shedding of flaming toroidal vortices. The flickering mechanism of interacting flames plays a crucial role in determining air entrainment, combustion rate, flame geometry, and products’ composition, etc. [10,11].

For a dual burner system that produces buoyancy-driven laminar flames, the flames generally exhibit an in-phase or antiphase flickering mode (with a constant phase difference of π) as shown in Fig. 1(a), depending on the burner separation distance (L) [8,12] or the gap flow behavior between the inner-side shear layers [13,14]. The transition (or phase-flip) point was identified at the critical burner separation distance (L_{crit}), which splits the two flickering modes and solely depends on the burner diameter (D) [15]; i.e., the two flames oscillate in an in-phase mode when $L < L_{\text{crit}}$ but an antiphase mode when $L > L_{\text{crit}}$. At $L = L_{\text{crit}}$, the flames exhibit an in-phase or antiphase mode unpredictably [15]. More interestingly, after the two flames are ignited at $L = L_{\text{crit}}$, a death mode shown in the left panel of Fig. 1(b) is temporarily generated due to time-delayed coupling of the two flames [16–24]. The death mode, also

termed “amplitude death,” is an abnormal flame behavior characterized by a cessation of flame flickering followed by steady-state burning, and is therefore preferable in practice (such as candle flames, Bunsen burner flames, and gas stove flames, etc.). However, the death mode shown in the left panel of Fig. 1(b) cannot self-sustain when the flames start to couple and gradually transitions to a flickering mode in an irreversible manner [as shown in Fig. 2(a)]; i.e., the flame behavior is uncontrollable at the critical burner separation distance.

In general, there are two ways to suppress flame flickering to generate a self-sustained death mode: one is reducing the buoyancy of flames (which can induce different modes of flame instabilities [11,25,26]) by lowering the fuel mass burning rate [as exemplified by the triple candle flames shown in the right panel of Fig. 1(b) [27] as well as in Refs. [28–30]] or creating a microgravity environment [31,32]; the other is reducing the kinematic viscosity of ambient air by decreasing the ambient pressure [31]. In this paper, we report a feasible way to generate a death mode in a dual burner system under normal gravity and atmospheric pressure without changing the fuel mass burning rate. Specifically, a criterion is deduced to prevent the coupling of the two flames by timeously varying their relative position around the critical burner separation distance (based on the theory of localized state control by periodic forcing [33–39]), thereby suppressing flame flickering and achieving steady-state combustion.

II. EXPERIMENTS

The current dual burner system is similar to that employed in our previous studies [14,15,40] and is schematically shown in Fig. 1(c), with more details given

*yuji@me.tut.ac.jp

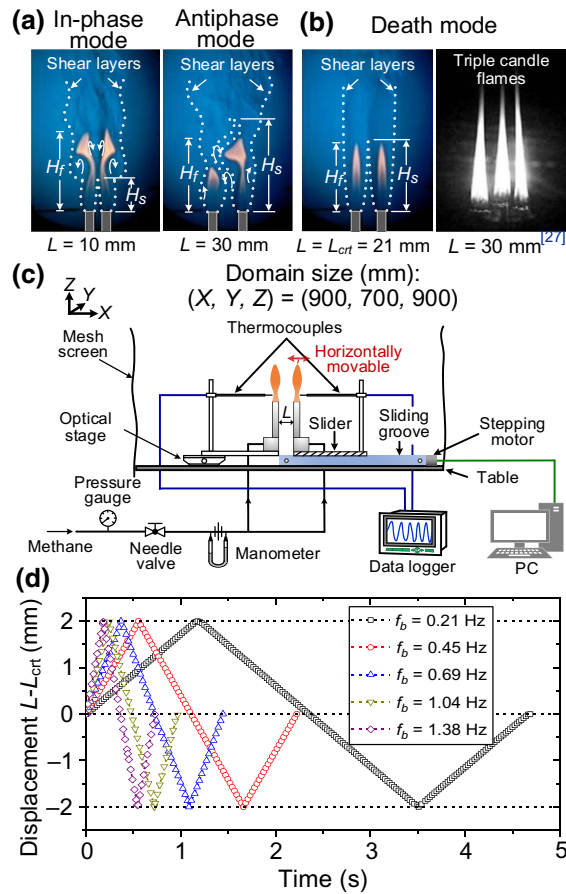


FIG. 1. The interaction of flames in a stationary dual burner system: (a) in-phase and antiphase flickering modes, and (b) a death mode. The interaction of flames in a moving dual burner system: (c) schematic view of the test setup, and (d) example burner displacement profiles ($L - L_{\text{crit}} = -2$ to 2 mm) at different moving frequencies.

in Appendix A. The only difference is that the burner on the right-hand side is endowed with an additional horizontal movement function here, such that it can move back and forth along the sliding groove around the critical burner separation distance at several displacement ranges ($L - L_{\text{crit}}$) and moving frequencies ($f_b = 1/T$, where T is the movement period of the burner). The values of $L - L_{\text{crit}}$ and f_b are detailed in Table I. At a certain burner moving velocity (v), different displacement ranges lead to different f_b . Based on the test results, it is found that the two flames no longer couple with each other when the moving velocity exceeds 11 mm/s, so the conditions of $v \leq 11$ mm/s are adopted. Example burner displacement profiles at different moving frequencies are depicted in Fig. 1(d), where $L - L_{\text{crit}}$ is from -2 to 2 mm. Meanwhile, the burner diameter and the flow rate of the fuel (methane gas with 99.9% minimum purity) for each burner are fixed to 10 mm and 500 mL/min, respectively, for reasons detailed in Appendix A.

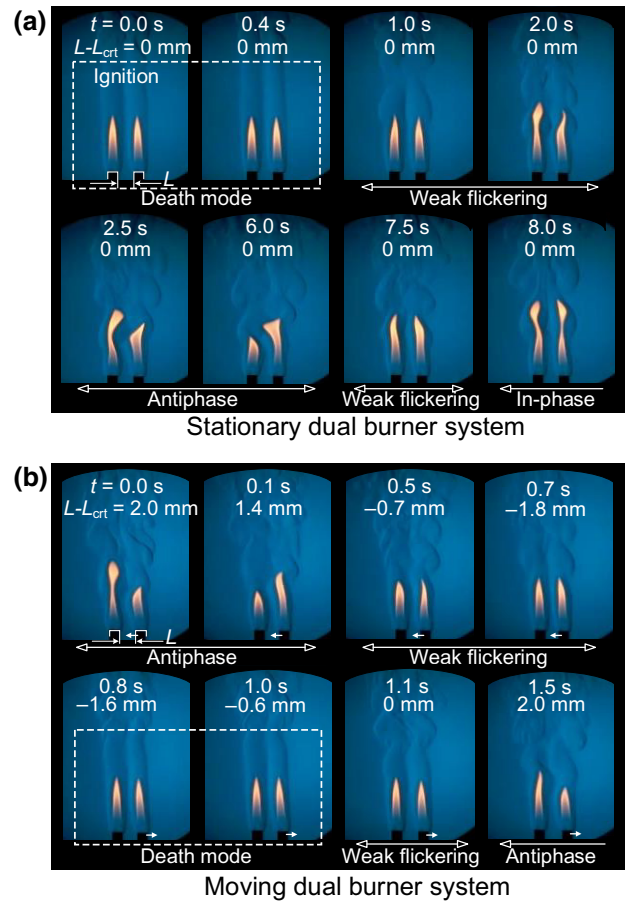


FIG. 2. Time-sequential images of the two flames: (a) in a stationary dual burner system with $L = L_{\text{crit}} = 21$ mm; (b) in a moving dual burner system with $L - L_{\text{crit}} = -2$ to 2 mm and $f_b = 0.69$ Hz (the burner on the right-hand side is a moving burner whose moving direction is indicated by a solid arrow).

III. RESULTS AND DISCUSSION

A. Stationary dual burner system

The time-sequential images of the two flames at the transition point in a stationary dual burner system (i.e., $L = L_{\text{crit}} = 21$ mm and $f_b = 0$ Hz) are shown in Fig. 2(a); note that the term “stationary” here means that the two

TABLE I. The moving frequency (f_b , Hz) of the movable burner under different displacement ranges ($L - L_{\text{crit}}$) and moving velocities (v).

v (mm/s)	$L - L_{\text{crit}}$ (mm)					
	(0, 2)	(-1, 2)	(-2, 2)	(-3, 2)	(-4, 2)	(-5, 2)
0.6	0.15	0.1	0.08	0.06	0.05	0.04
1.7	0.43	0.28	0.21	0.17	0.14	0.12
3.6	0.9	0.6	0.45	0.36	0.3	0.26
5.5	1.38	0.92	0.69	0.55	0.46	0.39
8.3	2.08	1.38	1.04	0.83	0.69	0.59
11	2.83	1.83	1.38	1.1	0.92	0.79

burners keep still when the flames interact. In the early stages after the two flames are ignited ($t \leq 0.4$ s), they present a nonflickering or death mode; as time goes by ($0.4 \text{ s} < t \leq 2.0$ s), a weak flickering mode appears, which then transitions to an antiphase mode ($2.0 \text{ s} < t \leq 6.0$ s), a weak flickering mode ($6.0 \text{ s} < t \leq 7.5$ s), and finally an in-phase mode ($t > 7.5$ s). These four coupling modes are differentiated by their characteristic flickering frequencies (f_c) determined using fast Fourier transform (FFT) analysis of the field temperature data; i.e., $f_c = 0$ Hz for a death mode, $0 < f_c < 10$ Hz for a weak flickering mode, $10 \leq f_c < 12$ Hz for an in-phase mode [15], and $f_c \geq 12$ Hz for an antiphase mode [15]. This phenomenon shows a heterogeneous and uncontrollable combustion state of the two flames at the transition point. In particular, the death mode cannot self-sustain due to buoyant acceleration [11,25]: the acceleration of buoyant plume gas in quiescent air causes the formation of toroidal vortices above the burner surface, which is regarded as the consequence of hydrodynamic shear instability driven by convective effects [31,41]. The slow-motion footage corresponding to Fig. 2(a) is shown in the Supplemental Material (Video 1) [42].

B. Moving dual burner system

For a moving dual burner system, Fig. 2(b) exemplifies the time-sequential flame images when the displacement range $L - L_{\text{crit}} = -2$ to 2 mm and the burner moving frequency $f_b = 0.69$ Hz. Note that the term “moving” here means that one of the two burners moves back and forth as the flames interact. It is seen that the flickering of the two flames is ceased during $t = 0.8\text{--}1.0$ s with a smooth shear layer around the flames, where the burner separation distance is shorter than the critical separation distance ($L_{\text{crit}} = 21$ mm). Besides $f_b = 0.69$ Hz, the death mode is also identified when $f_b = 0.45$ Hz, but not at other applied moving frequencies (where only the weak flickering mode is identified when $L < L_{\text{crit}}$). These facts suggest that the observed flame behavior is not in a quasisteady state, but a temporal state that strongly depends on the burner motion; i.e., the dynamic response of flame behavior to burner motion clearly exists. Additionally, different from the death mode shown in Fig. 2(a), the death mode in Fig. 2(b) can be always generated in each cycle of burner motion under these test conditions. The slow-motion test footage in one cycle of burner motion in the displacement range $L - L_{\text{crit}} = -2$ to 2 mm are provided in the Supplemental Material (Video 4) [42]; flame behaviors under three representative burner moving frequencies are shown to aid the understanding of these phenomena, including 0.08 Hz (without death mode), 0.69 Hz (with death mode), and 1.38 Hz (without death mode).

C. Characteristic flickering frequency

Figure 3 presents the variations of characteristic flame flickering frequency f_c with burner moving frequency (f_b)

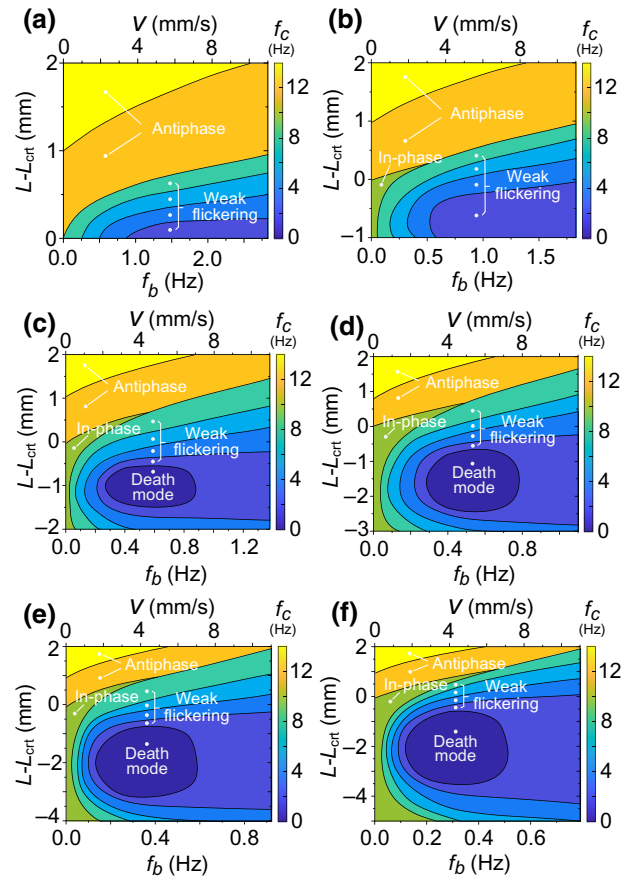


FIG. 3. Contour maps of f_c vs f_b in different displacement ranges ($L - L_{\text{crit}}$): (a) 0 to 2 mm; (b) -1 to 2 mm; (c) -2 to 2 mm; (d) -3 to 2 mm; (e) -4 to 2 mm; (f) -5 to 2 mm.

in different displacement ranges. It is worth noting that all the contour maps are drawn based on the flickering frequency data determined in half of a burner motion cycle (as exemplified in Appendix B). Moreover, the death mode regions shown in Fig. 3 are all controllable, so the transient death mode shown in Fig. 2(a) when $f_b = 0$ Hz is not included. It is seen that no death mode is identified in the displacement ranges of 0 to 2 mm and -1 to 2 mm. As the burner goes deeper into the region of $L < L_{\text{crit}}$ (i.e., the lower limit of $L - L_{\text{crit}}$ is smaller), the death mode region appears and gets larger, and naturally the duration of the death mode is extended. However, if the burner is moved further into this region, the two flames get closer, and the in-phase mode eventually becomes the dominant mode and the death mode region hardly expands [as shown in Figs. 3(e) and 3(f)]. These phenomena can be well understood by referring to the test footage in all the displacement ranges (Videos 2–7 in the Supplemental Material [42]).

D. Physical mechanism of the death mode

In essence, the flame coupling mode in a stationary dual burner system is governed by the gap flow behavior

between the two inner shear layers, resembling the transition mechanism from a stable to an unstable state in the development of a von Kármán vortex street [13–15]. When the burner separation distance is smaller than the critical separation distance, the shear layers around the flames [outlined with white dotted lines in the left panel of Fig. 1(a)] remain merged to cover the entire burner gap (i.e., the height of the inner shear layers H_s is lower than the free flame height H_f). Therefore, the air entrainment in the gap zone is effectively suppressed and the two flames driven by buoyant acceleration oscillate as a whole to exhibit symmetric vortices (namely, an in-phase mode). When the burner separation distance is increased, the entrained fresh air can penetrate the inner shear layers in the gap zone [i.e., H_s is larger than H_f as shown in the right panel of Fig. 1(a)] and the chance of air flow acceleration between the inner shear layers is promoted [14]. This would cause the meandering motion of the entrained air (showing a staggered vortex street), which in turn induces the two flames to exhibit an antiphase mode. At the critical separation distance between the two burners [where H_s is comparable to H_f as seen in the left panel of Fig. 1(b)], the buoyant acceleration temporarily ceases due to time-delayed coupling of the two flames to exhibit a death mode, resembling the amplitude death induced in coupled limit-cycle oscillators [16–24]. However, such a mode cannot self-sustain in a stationary dual burner system and transitions to a flickering mode over time with the coupling of the two flames [Fig. 2(a)].

In the moving dual burner system [Fig. 2(b)], the relative position of the two flames changes over time, so that they do not have enough time to couple in a fixed position; i.e., the flames are kept in a “to be coupled but not yet coupled” state. Then, a death mode can be induced if the burner configuration and its dynamic performance are appropriately designed (we will revisit this subsequently). The underlying physics is that the additional periodic forcing (driven by burner movement) can slow down the imminent critical transition in the transition phase [33–39], thereby maintaining the death mode for a certain time. Furthermore, it is worth noting that the response of flame behavior to burner motion is a dynamic process, so there must be a hysteresis to exhibit the drop in flickering frequency. This may explain the phenomenon observed in Fig. 3: different lower limits of each displacement range induce different local f_c values at the same burner separation distance (which is evident by comparing the contour maps displayed in Fig. 3). In other words, in order to map a complete death mode region, the moving burner should be as deep as possible into the region of $L < L_{\text{crit}}$ [see Fig. 3(f)].

Additionally, the death mode in the moving dual burner system can sustain for a period of time in each burner motion cycle. The shear layer evolution time (approximately 1 s) is estimated by H_f/u_F , where u_F is the fuel jet velocity (106 mm/s) and H_f is 100 mm, as detailed in

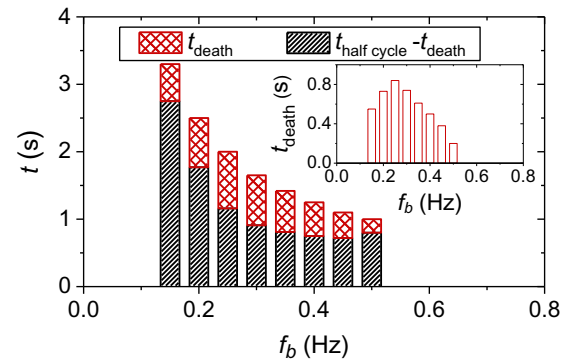


FIG. 4. Duration of the death mode in the displacement range of $L - L_{\text{crit}} = -5$ to 2 mm (where $t_{\text{half cycle}}$ is the moving time of the burner in half of a burner motion cycle).

Appendix A. The death mode only appears in an intermediate range of f_b (Fig. 3), because (1) if f_b is lower than this range, the residence time of the moving burner in the transition phase is longer than the coupling delay time of the two flames, and they start to couple in such a region; and (2) if f_b is higher than this range, the residence time of the moving burner in the transition phase is shortened and the separation distance between the two burners greatly shifts in a shear layer evolution period, so the two flames tend to be decoupled. This is further confirmed by Fig. 4, which illustrates the duration of the death mode (t_{death}) in the displacement range of $L - L_{\text{crit}} = -5$ to 2 mm (where the most complete death mode region is obtained) calculated based on Fig. 3. It is seen that t_{death} reaches its peak value (0.84 s) at $f_b = 0.25$ Hz; this is smaller than the shear layer evolution time (1 s), suggesting the death mode is generated within a shear layer evolution period. These facts indicate that only in an intermediate range of f_b can the burner motion keep pace with the evolution of shear layers, thereby successfully generating a death mode in a moving dual burner system.

E. Criterion to map a death mode region

Next, scaling analysis is performed to study the parameters that govern the characteristic flame flickering frequency (f_c). Two nondimensional quantities, $\alpha \text{Gr}^{1/2}$ and $f_b \Delta L / (gD)^{1/2}$, are deduced to quantify the burner configuration and its dynamic performance, respectively, where $\alpha = L/D$, with D the burner diameter, and $\text{Gr} (= gD^3/\nu_a^2)$, with g the acceleration due to gravity and ν_a the kinematic viscosity of ambient air. The scaling analysis of characteristic flickering frequency of the two flames is detailed in Appendix C. Figure 5 plots the variation of the normalized characteristic flickering frequency f_c/f_s with $\alpha \text{Gr}^{1/2}$ and $f_b \Delta L / (gD)^{1/2}$ based on the data shown in Fig. 3(f) (where the most complete death mode region is obtained); f_s is the frequency of a single flickering flame determined in this study. It is seen that the death mode

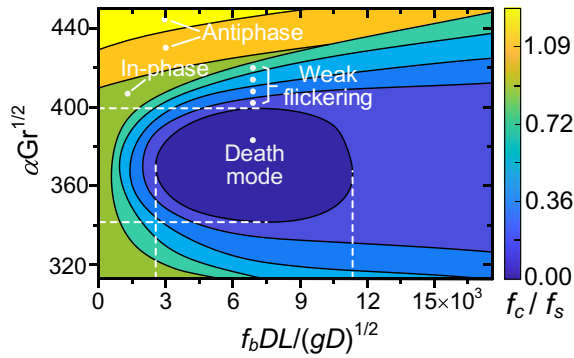


FIG. 5. The variation of normalized characteristic flickering frequency f_c/f_s with dimensionless burner configuration $\alpha Gr^{1/2}$ and dimensionless burner moving velocity $f_b \Delta L / (gD)^{1/2}$ in the displacement range $L - L_{\text{crit}} = -5$ to 2 mm.

is located in the region of $341.8 < \alpha Gr^{1/2} < 399.5$ and $2.6 \times 10^{-3} < f_b \Delta L / (gD)^{1/2} < 1.14 \times 10^{-2}$. The range of $\alpha Gr^{1/2}$ pertains to the transition phase between in-phase and antiphase modes identified in Ref. [13], where $\alpha Gr^{1/2}$ ranges from 300 to 420 for various burner diameters and separation distances. In addition, suppose there is a buoyant diffusion flame with the same free flame height as in this study but a larger (smaller) burner diameter D ; its heat release rate must be higher (lower) than the current flame according to the quantitative relationship between flame height and burner diameter. As a result, the moving velocity of the burner ($2f_b \Delta L$) must be increased (decreased) to generate a death mode, and the value of $f_b \Delta L / (gD)^{1/2}$ would still fall into the current range. The underlying reason may be that the flame's transition from death mode to flickering mode depends on the foregoing interaction of the two inner shear layers, the thickness of which remains constant for a death mode regardless of how the burner diameter changes (as clarified in Appendix C). It is considered that these disclosed ranges could serve as general criteria to map a complete death mode region generated by dual buoyant diffusion flames with different burner configurations and dynamic performances. In short, the scaling model deduced previously provides a feasible way to generate nonflickering flames in a moving dual burner system under normal gravity and atmospheric pressure without changing the fuel mass burning rate. This would have some implications for both academic research and industrial applications in the fields of nonlinear physics and combustion technology.

IV. SUMMARY

In summary, this study provides a feasible way to suppress flame flickering, namely to generate a death mode in a dual burner system under normal gravity and atmospheric pressure without changing the fuel mass burning rate, thereby achieving steady-state combustion. It is

considered that the reciprocating motion of the burner can keep the two flames in a “to be coupled but not yet coupled” state by timeously varying their relative position at the transition phase between in-phase and antiphase flickering modes. If the burner motion can keep pace with the evolution of shear layers, a death mode is generated. This phenomenon is well clarified based on the theory of localized state control using periodic forcing. Furthermore, the criterion to map a complete death mode region in a moving dual burner system is defined by two dimensionless parameters, $\alpha Gr^{1/2}$ and $f_b \Delta L / (gD)^{1/2}$, which quantify the burner configuration and its dynamic performance, respectively. A systematic numerical modeling, combining the theories of linear stability analysis, periodic forcing effect, and time-delay interaction of limit-cycle oscillators, etc., will be conducted in our future work to quantify the suppression mechanism of flame flickering in a moving dual burner system.

ACKNOWLEDGMENTS

The authors thank Mr. Keisuke Mochizuki for his initial effort on this project and the financial support from the Toyota Physical and Chemical Research Institute.

APPENDIX

Additional information on the experimental setup details, the determination of the characteristic flickering frequency of the two flames, and the scaling analysis of characteristic flickering frequency of the two flames are provided in Appendices A, B, and C, respectively.

APPENDIX A: EXPERIMENTAL SETUP DETAILS

The test configuration in this work is basically the same as that in our previous work [14,15,40] except for the horizontal movement performance of the right-hand side burner [see Fig. 1(c) in the article]. The flow rate of the fuel (methane gas with 99.9% minimum purity) for each burner is fixed at 500 mL/min because the transition point between in-phase and antiphase modes has been demonstrated to be insensitive to the fuel flow rate in the range from 500 to 3500 mL/min [15]; the underlying reason is that for buoyant diffusion flames with low fuel flow rates, the flickering frequency is basically independent of fuel flow rate (or fuel jet velocity) [31,43]. As shown in Fig. 6(a), the thickness of the inner shear layers δ_{crit} is constant (about 14 mm) at the transition point for various burner diameters [44], so the cylindrical nozzle (inner) diameter (D) is fixed to 10 mm in this study and the corresponding free flame height (H_f) is about 100 mm. The fuel Froude number is far less than 1, suggesting the two flames are buoyancy driven. The critical burner separation distance (L_{crit}) at the transition point is 21 mm when $D = 10$ mm [14,15]. The two flames are generated in a space ($900 \times 700 \times 900$ mm in size) under atmospheric

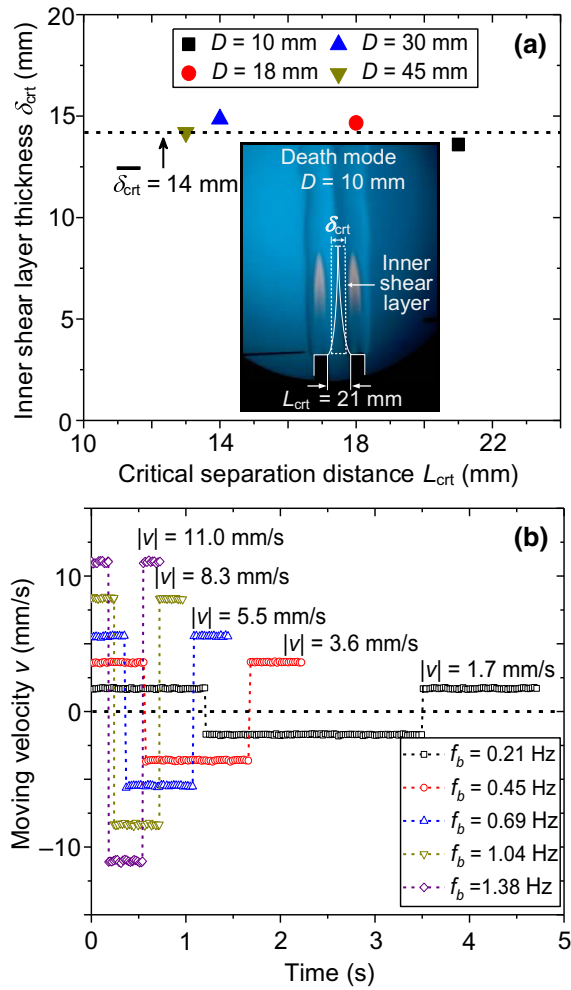


FIG. 6. (a) Variation of inner shear layer thickness (δ_{crit}) with critical burner separation distance (L_{crit}) when death modes are temporarily generated in stationary dual burner systems under different burner diameters ($D = 10$ – 45 mm) [44]; (b) moving velocity profiles of the movable burner corresponding to different moving frequencies shown in Fig. 1(d).

pressure, and surrounded by a mesh screen (to suppress any interference from the ambient). One burner is fixed on the optical stage, while the other is mounted on a moving slider controlled by a stepping motor (Oriental Motor, model AZM46AC), which can make periodic reciprocating movements along the sliding groove. Two thermocouples (K type; referred to as TC hereafter; 0.25 mm in junction diameter) are placed near the burner exit to monitor the variation of field temperature outside the flame body with time at a sampling rate of 10 ms; the TC signal is then processed based on FFT to obtain the characteristic flickering frequency of the flames. The flame behavior is recorded by a high-speed camera (Casio EX-F1) with 300 frames/s frame rate and 512×384 pixels in resolution. Schlieren imaging is also employed to visualize the flames and hot plume through shadows of varying density formed around the flames.

In the experiment, the right-hand side burner [as shown in Fig. 1(c)] moves back and forth along the sliding groove around the critical burner separation distance at several ranges of displacement ($L - L_{\text{crit}}$) and moving frequencies ($f_b = 1/T$, where T is the movement period of the burner). The moving velocity profiles corresponding to Fig. 1(d) are depicted in Fig. 6(b), where the displacement range is from -2 to 2 mm.

APPENDIX B: DETERMINATION OF CHARACTERISTIC FLICKERING FREQUENCY

The two flames synchronize with each other and have the same flickering frequency, so the temperature data captured by either of the two TCs are selected for FFT analysis. Figure 7 exemplifies the temperature profile in one cycle of burner motion when the burner displacement range $L - L_{\text{crit}} = -2$ to 2 mm and burner moving frequency $f_b = 0.69$ Hz. The death mode is identified when the twin burners are moving away from each other [Fig. 2(b)], so the temperature data of the right half region of Fig. 7 are used for analysis. This region is divided into eight time domains by the blue dotted lines at intervals of $L - L_{\text{crit}} = 0.5$ mm. For each time domain, there are only about nine data points and the corresponding FFT resolution is around 2.8 Hz in the frequency domain from 0 to 25 Hz. According to previous studies [13,15], a frequency resolution of at least 0.1 Hz should be ensured. We further increase the number of data points in each time domain from 9 to 256 based on the concept of zero padding [45]; therefore, the resulting frequency resolution is approximately 0.1 Hz.

FFT analysis is performed for each zero-padded time domain, and the results are displayed in Fig. 8. From the peak point on each spectrum, the characteristic flickering

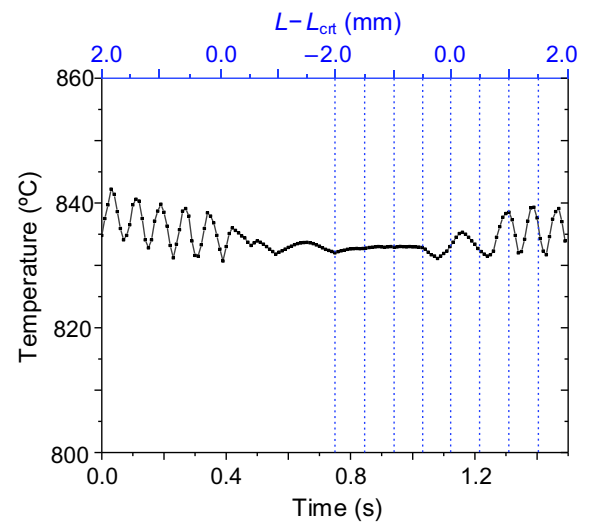


FIG. 7. Temperature data in one burner motion cycle with $L - L_{\text{crit}} = -2$ to 2 mm and $f_b = 0.69$ Hz.

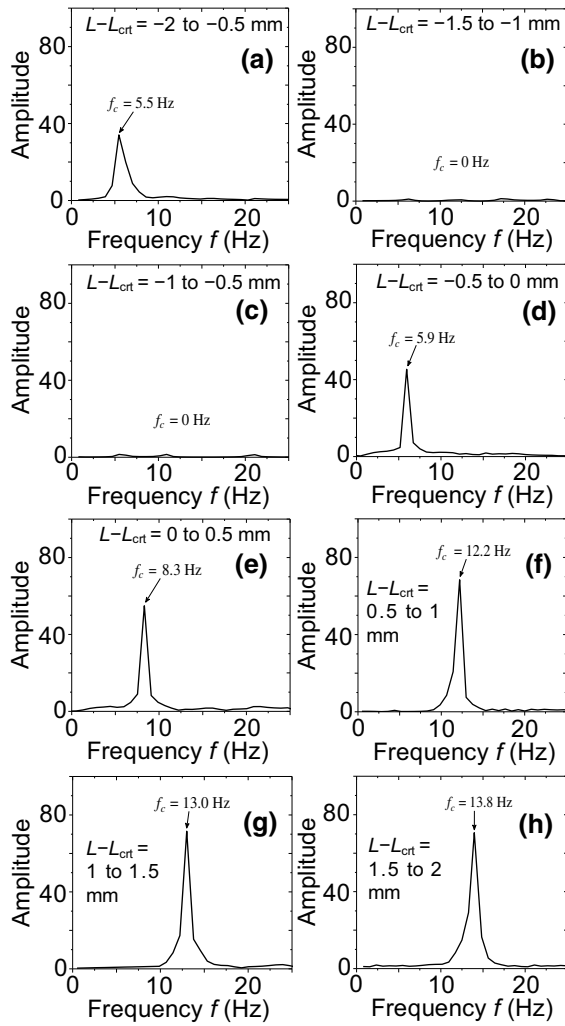


FIG. 8. FFT analysis results at different burner positions (or time domains) in one cycle of burner motion with $L - L_{\text{crit}} = -2$ to 2 mm and $f_b = 0.69$ Hz.

frequency of the flames (f_c) in the corresponding burner position is determined. f_c is regarded as 0 Hz when there is no apparent peak on the spectrum as shown in Figs. 8(b) and 8(c). With the same method, f_c in other cases of $L - L_{\text{crit}}$ and f_b are also obtained. The contour maps of f_c against f_b in different displacement ranges are shown in Fig. 3.

APPENDIX C: SCALING ANALYSIS OF CHARACTERISTIC FLICKERING FREQUENCY

Based on the phenomenological observations and physical understanding disclosed in this work, as well as our previous studies [14,15], f_c is determined by the burner diameter D , gravity g , the kinematic viscosity of ambient air ν_a , the separation distance between the two flames L , the length of the displacement range ΔL , and the moving

frequency of the burner f_b , i.e.,

$$f_c = f(D, g, \nu_a, L, \Delta L, f_b). \quad (\text{C1})$$

Based on the Π theorem of dimensional analysis [46], Eq. (C1) can then be rearranged as

$$\frac{f_c}{f_b} = f\left(\frac{L}{D}, \frac{\sqrt{gD^3}}{\nu_a}, \frac{f_b \Delta L}{\sqrt{gD}}\right) = f\left(\alpha, \text{Gr}^{1/2}, \frac{f_b \Delta L}{\sqrt{gD}}\right), \quad (\text{C2})$$

where f_s is the frequency of a single flickering flame determined in this study [which is scaled by $(g/D)^{1/2}$ [13]], $\alpha = L/D$, and $\text{Gr}(= gD^3/\nu_a^2)$ is the Grashof number [13,47] measuring the relative effects between buoyant acceleration and viscous forces. Note that the combination of α and Gr , namely $\alpha \text{Gr}^{1/2}$, has been proved to serve as a general criterion to predict the flickering mode transition in a stationary dual burner system [13]. $f_b \Delta L / (gD)^{1/2}$ is a nondimensional velocity, which is proportional to the moving velocity of the burner $v = 2f_b \Delta L$ (Table I) and thus facilitates the definition of two limiting cases, namely $v = 0$ (the demarcation point between stationary and moving dual burner systems) and $v = 11$ mm/s (the demarcation point of flame coupling and noncoupling in a moving dual burner system determined in this study). In short, $\alpha \text{Gr}^{1/2}$ quantifies the burner configuration (L and D), while $f_b \Delta L / (gD)^{1/2}$ characterizes its dynamic performance (v).

- [1] M. Faraday, W. Crookes, and P. Rossiter, *The chemical history of a candle* (Crowell, New York, 1957).
- [2] D. Durao and J. H. Whitelaw, Instantaneous velocity and temperature measurements in oscillating diffusion flames, *Proc. R. Soc. London, Ser. A* **338**, 479 (1974).
- [3] A. J. Grant and J. M. Jones, Low-frequency diffusion flame oscillations, *Combust. Flame* **25**, 153 (1975).
- [4] T. Maxworthy, The flickering candle: transition to a global oscillation in a thermal plume, *J. Fluid Mech.* **390**, 297 (1999).
- [5] J. Buckmaster and N. Peters, The infinite candle and its stability—a paradigm for flickering diffusion flames, *Symp. (Int.) Combust.* **21**, 1829 (1988).
- [6] D. M. Forrester, Arrays of coupled chemical oscillators, *Sci. Rep.* **5**, 16994 (2015).
- [7] S. Dange, S. A. Pawar, K. Manoj, and R. I. Sujith, Role of buoyancy-driven vortices in inducing different modes of coupled behaviour in candle-flame oscillators, *AIP Adv.* **9**, 015119 (2019).
- [8] H. Kitahata, J. Taguchi, M. Nagayama, T. Sakurai, Y. Ikura, A. Osa, Y. Sumino, M. Tanaka, E. Yokoyama, and H. Miike, Oscillation and synchronization in the combustion of candles, *J. Phys. Chem. A* **113**, 8164 (2009).
- [9] A. Putnam and C. Speich, A model study of the interaction of multiple turbulent diffusion flames, *Symp. (Int.) Combust.* **9**, 867 (1963).

- [10] A. Hamins, J. Yang, and T. Kashiwagi, An experimental investigation of the pulsation frequency of flames, *Symp. (Int.) Combust.* **24**, 1695 (1992).
- [11] B. M. Cetegen and T. A. Ahmed, Experiments on the periodic instability of buoyant plumes and pool fires, *Combust. Flame* **93**, 157 (1993).
- [12] T. Y. Toong, R. F. Salant, J. M. Stopford, and G. Y. Anderson, *Symp. (Int.) Combust* **10**, 1301 (1965).
- [13] T. Yang, X. Xia, and P. Zhang, Vortex-dynamical interpretation of anti-phase and in-phase flickering of dual buoyant diffusion flames, *Phys. Rev. Fluids* **4**, 053202 (2019).
- [14] A. Bunkwang, T. Matsuoka, and Y. Nakamura, Similarity of dynamic behavior of buoyant single and twin jet-flame(s), *J. Therm. Sci. Technol.* **15**, JTST0028 (2020).
- [15] A. Bunkwang, T. Matsuoka, and Y. Nakamura, Mode transition of interacting buoyant non-premixed flames, *J. Therm. Sci. Technol.* **15**, JTST0003 (2020).
- [16] G. Saxena, A. Prasad, and R. Ramaswamy, Amplitude death: The emergence of stationarity in coupled nonlinear systems, *Phys. Rep.* **521**, 205 (2012).
- [17] R. Herrero, M. Figueras, J. Rius, F. Pi, and G. Orriols, Experimental Observation of the Amplitude Death Effect in Two Coupled Nonlinear Oscillators, *Phys. Rev. Lett.* **84**, 5312 (2000).
- [18] D. R. Reddy, A. Sen, and G. L. Johnston, Time Delay Induced Death in Coupled Limit Cycle Oscillators, *Phys. Rev. Lett.* **80**, 5109 (1998).
- [19] F. M. Atay, Distributed Delays Facilitate Amplitude Death of Coupled Oscillators, *Phys. Rev. Lett.* **91**, 094101 (2003).
- [20] S. Mizukami, K. Konishi, Y. Sugitani, T. Kouda, and N. Hara, Effects of frequency mismatch on amplitude death in delay-coupled oscillators, *Phys. Rev. E* **104**, 054207 (2021).
- [21] W. Zou and M. Zhan, Partial time-delay coupling enlarges death island of coupled oscillators, *Phys. Rev. E* **80**, 065204 (2009).
- [22] T. Biwa, S. Tozuka, and T. Yazaki, Amplitude Death in Coupled Thermoacoustic Oscillators, *Phys. Rev. Appl.* **3**, 034006 (2015).
- [23] T. Biwa, Y. Sawada, H. Hyodo, and S. Kato, Suppression of Spontaneous Gas Oscillations by Acoustic Self-Feedback, *Phys. Rev. Appl.* **6**, 044020 (2016).
- [24] A. Sahay, A. Roy, S. A. Pawar, and R. I. Sujith, Dynamics of Coupled Thermoacoustic Oscillators Under Asymmetric Forcing, *Phys. Rev. Appl.* **15**, 044011 (2021).
- [25] B. Cetegen and Y. Dong, Experiments on the instability modes of buoyant diffusion flames and effects of ambient atmosphere on the instabilities, *Exp. Fluids* **28**, 546 (2000).
- [26] M. C. Rogers and S. W. Morris, Buoyant Plumes and Vortex Rings in an Autocatalytic Chemical Reaction, *Phys. Rev. Lett.* **95**, 024505 (2005).
- [27] K. Okamoto, A. Kijima, Y. Umeno, and H. Shima, Synchronization in flickering of three-coupled candle flames, *Sci. Rep.* **6**, 36145 (2016).
- [28] K. Manoj, S. A. Pawar, and R. I. Sujith, Experimental evidence of amplitude death and phase-flip bifurcation between in-phase and anti-phase synchronization, *Sci. Rep.* **8**, 11626 (2018).
- [29] K. Manoj, S. A. Pawar, S. Dange, S. Mondal, R. I. Sujith, E. Surovyatkina, and J. Kurths, Synchronization route to weak chimera in four candle-flame oscillators, *Phys. Rev. E* **100**, 062204 (2019).
- [30] K. Manoj, S. A. Pawar, and R. I. Sujith, Experimental investigation on the susceptibility of minimal networks to a change in topology and number of oscillators, *Phys. Rev. E* **103**, 022207 (2021).
- [31] D. Durox, T. Yuan, and E. Villermaux, The effect of buoyancy on flickering in diffusion flames, *Combust. Sci. Technol.* **124**, 277 (2007).
- [32] R. W. Davis and E. F. Moore, Preliminary results of a numerical-experimental study of the dynamic structure of a buoyant jet diffusion flame, *Combust. Flame* **83**, 263 (1991).
- [33] J. Baillieul, *Dynamics and Control of Mechanical Systems: The Falling Cat and Related Problems* (American Mathematical Society, Providence, RI, USA, 1993), pp. 1–23.
- [34] L. Glass and J. Sun, Periodic forcing of a limit-cycle oscillator: Fixed points, Arnold tongues, and the global organization of bifurcations, *Phys. Rev. E* **50**, 5077 (1994).
- [35] M. Belhaq and M. Houssni, Quasi-periodic oscillations, chaos and suppression of chaos in a nonlinear oscillator driven by parametric and external excitations, *Nonlinear Dyn.* **18**, 1 (1999).
- [36] M. G. Clerc, F. Haudin, S. Residori, U. Bortolozzo, and R. G. Rojas, Control and managing of localized states in two-dimensional systems with periodic forcing, *Eur. Phys. J. D* **59**, 43 (2010).
- [37] W. Kurebayashi, S. Shirasaka, and H. Nakao, Phase Reduction Method for Strongly Perturbed Limit Cycle Oscillators, *Phys. Rev. Lett.* **111**, 214101 (2013).
- [38] J. Ma, Y. Xu, W. Xu, Y. Li, and J. Kurths, Slowing down critical transitions via Gaussian white noise and periodic force, *Sci. China: Technol. Sci.* **62**, 2144 (2019).
- [39] B. Wallace, L. W. Kong, A. Rodriguez, and Y. C. Lai, Synchronous Transition in Complex Object Control, *Phys. Rev. Appl.* **16**, 034012 (2021).
- [40] M. Mochizuki, T. Matsuoka, and Y. Nakamura, Study on oscillation and transition behavior of interacting flickering flames, *Bull. Jpn. Assoc. Fire Sci. Eng.* **67**, 21 (2017).
- [41] P. Huerre and P. A. Monkewitz, Local and global instabilities in spatially developing flows, *Annu. Rev. Fluid Mech.* **22**, 473 (1990).
- [42] See Supplemental Material at <http://link.aps.org/supplemental/10.1103/PhysRevApplied.19.014060> for videos showing the flame behaviors in the stationary and moving dual burner systems.
- [43] A. Lingers, M. Reeker, and M. Schreiber, Instability of buoyant diffusion flames, *Exp. Fluids* **20**, 241 (1996).
- [44] A. Bunkwang, *Study on flickering behavior of interacting two jet diffusion flames* (Department of Mechanical Engineering, Toyohashi University of Technology, Toyohashi, Aichi, Japan, 2021).
- [45] S. Hilbert, FFT Zero Padding. <https://www.bitweenie.com/listings/fft-zero-padding/>, (accessed Nov. 18 2021).
- [46] E. Buckingham, On physically similar systems; illustrations of the use of dimensional equations, *Phys. Rev.* **4**, 345 (1914).
- [47] C. K. Law, *Combustion physics* (Cambridge university press, Cambridge, UK, 2010).